AJNR

Correlation of Tumor Immunohistochemistry with Dynamic Contrast-Enhanced and DSC-MRI Parameters in Patients with Gliomas

T.B. Nguyen, G.O. Cron, K. Bezzina, K. Perdrizet, C.H. Torres, S. Chakraborty, J. Woulfe, G.H. Jansen, R.E. Thornhill, B. Zanette and I.G. Cameron

AJNR Am J Neuroradiol 2016, 37 (12) 2217-2223
doi: https://doi.org/10.3174/ajnr.A4908
http://www.ajnr.org/content/37/12/2217

Correlation of Tumor Immunohistochemistry with Dynamic Contrast-Enhanced and DSC-MRI Parameters in Patients with Gliomas

T.B. Nguyen, G.O. Cron, K. Bezzina, K. Perdrizet, C.H. Torres, S. Chakraborty, J. Woulfe, G.H. Jansen, R.E. Thornhill, B. Zanette, and I.G. Cameron

ABSTRACT

BACKGROUND AND PURPOSE: Tumor CBV is a prognostic and predictive marker for patients with gliomas. Tumor CBV can be measured noninvasively with different MR imaging techniques; however, it is not clear which of these techniques most closely reflects histologically-measured tumor CBV. Our aim was to investigate the correlations between dynamic contrast-enhanced and DSC-MR imaging parameters and immunohistochemistry in patients with gliomas.

MATERIALS AND METHODS: Forty-three patients with a new diagnosis of glioma underwent a preoperative MR imaging examination with dynamic contrast-enhanced and DSC sequences. Unnormalized and normalized cerebral blood volume was obtained from DSC MR imaging. Two sets of plasma volume and volume transfer constant maps were obtained from dynamic contrast-enhanced MR imaging. Plasma volume obtained from the phase-derived vascular input function and bookend T1 mapping (Vp_Φ) and volume transfer constant obtained from phase-derived vascular input function and bookend T1 mapping (K^{trans}_Φ) were determined. Plasma volume obtained from magnitude-derived vascular input function (Vp_SI) and volume transfer constant obtained from magnitude-derived vascular input function (K^{trans}_SI) were acquired, without T1 mapping. Using CD34 staining, we measured microvessel density and microvessel area within 3 representative areas of the resected tumor specimen. The Mann-Whitney *U* test was used to test for differences according to grade and degree of enhancement. The Spearman correlation was performed to determine the relationship between dynamic contrast-enhanced and DSC parameters and histopathologic measurements.

RESULTS: Microvessel area, microvessel density, dynamic contrast-enhanced, and DSC-MR imaging parameters varied according to the grade and degree of enhancement ($P < .05$). A strong correlation was found between microvessel area and Vp_Φ and between microvessel area and unnormalized blood volume ($r_s \geq 0.61$). A moderate correlation was found between microvessel area and normalized blood volume, microvessel area and Vp_SI, microvessel area and K^{trans}_Φ, microvessel area and K^{trans}_SI, microvessel density and Vp_Φ, microvessel density and unnormalized blood volume, and microvessel density and normalized blood volume ($0.44 \leq r_s \leq 0.57$). A weaker correlation was found between microvessel density and K^{trans}_Φ and between microvessel density and K^{trans}_SI ($r_s \leq 0.41$).

CONCLUSIONS: With dynamic contrast-enhanced MR imaging, use of a phase-derived vascular input function and bookend T1 mapping improves the correlation between immunohistochemistry and plasma volume, but not between immunohistochemistry and the volume transfer constant. With DSC-MR imaging, normalization of tumor CBV could decrease the correlation with microvessel area.

ABBREVIATIONS: DCE = dynamic contrast-enhanced; K^{trans} = volume transfer constant; MVA = microvessel area; MVD = microvessel density; Φ = phase-derived vascular input function and bookend T1 mapping; rCBV = ratio of tumor blood volume and normal-appearing contralateral white matter blood volume (also known as relative blood volume or normalized blood volume); r_s = Spearman rank correlation coefficient; SI = magnitude-derived signal intensity; uCBV = unnormalized tumor blood volume (ie, the CBV not divided by the value in contralateral white matter); VIF = vascular input function; Vp = plasma volume

Tumor CBV has been found to be a prognostic and predictive marker for patients with gliomas.[1-5] Measurements of blood volume can be obtained by using dynamic contrast-enhanced (DCE) MR imaging or dynamic susceptibility contrast MR imaging. Both techniques have their own advantages and disadvantages.

Received February 20, 2016; accepted after revision July 1.

From the Departments of Radiology (T.B.N., G.O.C., C.H.T., R.E.T., I.G.C., S.C.), Medical Physics (I.G.C.), Pathology (G.H.J., J.W.), Internal Medicine (K.P.), and Psychiatry (K.B.), The Ottawa Hospital, University of Ottawa, The Ottawa Hospital Research Institute, Ottawa, Ontario, Canada; and Department of Medical Biophysics (B.Z.), University of Toronto, Toronto, Ontario, Canada.

This work was supported by an investigator-initiated research grant from Bayer Healthcare.

Abstract previously presented at: Annual Meeting of the American Society of Neuroradiology and the Foundation of the ASNR Symposium, April 25–30, 2015; Chicago, Illinois.

Please address correspondence to Thanh Binh Nguyen, MD, Department of Radiology, The Ottawa Hospital, 1053 Carling Ave, Ottawa, ON, K1Y 4E9, Canada; e-mail: thnguyen@toh.on.ca

http://dx.doi.org/10.3174/ajnr.A4908

DSC-MR imaging can provide a semiquantitative measurement of cerebral blood volume, but measurement reliability depends on image acquisition and postprocessing approaches such as normalization techniques.[6] DCE-MR imaging requires an accurate measurement of the vascular input function (VIF) and T1 mapping for absolute quantification of the plasma volume (Vp) and volume transfer constant (K^{trans}).[7] Recently, phase-based VIFs have been used in DCE-MR imaging to circumvent the limitations of magnitude-based VIFs, such as signal saturation and inflow artifacts.[8-11] MR imaging signal data are complex numbers, composed of magnitude and phase. The magnitude is the strength of the signal and is affected by T1, T2, proton density, inflow, and magnetic field inhomogeneity. The phase is an angle that is proportional to the nuclear MR frequency of the signal. In routine clinical MR imaging, images are composed of just the magnitude, with the phase discarded. Contrast agents change the nuclear MR frequency (and therefore the phase) of nearby tissue via a physical, spatial effect, which depends only on the contrast agent concentration and the geometry of the nearby tissue. In blood vessels running parallel with the main magnetic field, the relationship between phase and concentration is linear and can be calculated from first principles. The magnitude part of the signal, on the other hand, saturates at a high concentration and can be severely affected by inflow. The phase, therefore, has the potential to provide more reliable measures of the arterial input function than the magnitude.

To our knowledge, correlation between DCE-MR imaging–derived parameters by using phase-derived VIFs with microvessel density (MVD) and microvessel area (MVA) from immunohistochemistry has not been investigated in patients with gliomas. The purpose of this study was to investigate the correlations among MR imaging contrast enhancement, DSC parameters, DCE parameters, and immunohistochemistry, by using both phase-derived VIFs (with T1 mapping) and magnitude-derived VIFs (without T1 mapping).

MATERIALS AND METHODS

Patient Population

All examinations were conducted in accordance with the guidelines of The Ottawa Hospital for human research, and written informed consent was obtained from all participating subjects. From March 1, 2011, to December 31, 2013, 70 consecutive patients presenting at The Ottawa Hospital with a newly diagnosed brain lesion compatible with a glioma were asked to participate in this study. These patients were part of a diagnostic accuracy study on DCE- and DSC-MR imaging for glioma grading, which has been published previously.[11] Eleven patients were excluded due to the absence of a histopathologic diagnosis or the presence of an alternate histopathologic diagnosis: no biopsy ($n = 2$), inconclusive biopsy ($n = 1$), metastatic disease ($n = 2$), lymphomas ($n = 2$), glioneuronal tumors ($n = 2$), meningioma ($n = 1$), and neurosarcoidosis ($n = 1$). Nine patients with gliomas were excluded for technical reasons: inadequate bolus injection of contrast ($n = 4$), hemorrhage within the glioblastoma causing extensive susceptibility artifacts ($n = 3$), dynamic acquisition not centered over the tumor ($n = 1$), and inadequate VIF for the DCE acquisition ($n = 1$). Seven more patients were excluded because of a very small biopsy specimen or unspecific background CD34 staining.

MR Imaging Acquisition Protocols

Conventional MR imaging was performed on a 3T scanner (Magnetom Trio; Siemens, Erlangen, Germany) by using axial T1-weighted precontrast (TR = 280 ms, TE = 2.51 ms, thickness = 3 mm), axial FLAIR (TR = 9710 ms, TE = 93 ms, TI = 2580 ms, thickness = 3 mm), axial T2-weighted (TR = 6910 ms, TE = 97 ms, thickness = 3 mm), axial T1 volumetric interpolated brain examination postcontrast (TR = 8.48 ms, TE = 3.21 ms, flip angle = 12°, thickness = 1 mm), and coronal T1-weighted postcontrast (TR = 280 ms, TE = 2.51 ms, thickness = 4 mm) images.

DCE-MR imaging was performed by using a 3D FLASH sequence (TR = 6.5 ms, TE = 1.7/3.9 ms, flip angle = 30°, thickness = 5 mm, 18 sections, temporal resolution = 3.5 seconds, duration = 440 seconds). This pulse sequence generated phase images in addition to the standard magnitude images. Both before and after the dynamic scan, two 3D volumetric interpolated brain examination sequences with different flip angles (TR = 20 ms, TE = 1.22 ms, flip angle = 4° and 25°, thickness = 5 mm, 18 sections) were acquired, which enabled calculation of the T1 maps.

In patients weighing between 50 and 100 kg, a fixed preloaded dose of 0.05 mmol (equivalent to 5 mL) of Gadovist 1.0 (Bayer Schering Pharma, Berlin, Germany) was injected at 2 mL/s for DCE imaging. This also served to decrease the T1 effects before a second injection of 0.05 mmol of contrast was performed for the DSC perfusion imaging. In patients weighing <50 kg or >100 kg, we used a dose of 0.05 mmol/kg.

The second injection of contrast agent was given 10 minutes after the first injection at 4 mL/s. DSC imaging was performed by using a T2* EPI gradient recalled-echo sequence (TR = 2380 ms, TE = 54 ms, flip angle = 90°, thickness = 5 mm, 18 sections, temporal resolution = 2.5 seconds, duration = 125 seconds). Seven baseline measurements were obtained before contrast injection.

Postprocessing of DCE Images

Two methods were used to process the DCE images. The extended Tofts model was used in both cases.

Phase-Derived Vascular Input Function with Bookend T1 Correction. Voxelwise maps of tissue contrast concentration across time were calculated by using pre- and post-DCE T1 maps combined with the tissue signal-intensity-versus-time curve.[12] Phase analysis was used to estimate the VIF from 1 section where the superior sagittal sinus ran approximately parallel with the main magnetic field and perpendicular to the section. A small ROI (2–4 pixels) was drawn at the center of the superior sagittal sinus, and the mean phase was measured as a function of time. The phase-versus-time curve was converted to a gadolinium-versus-time curve, which was then saved in a text file. This step was performed off-line by using in-house software written in IDL (Exelis Visual Information Solutions, Boulder, Colorado) and has been described in previous articles.[10,11] The gadolinium-versus-time curve was imported as the VIF in a kinetic modeling-analysis software (nordicICE software, Version 2; NordicNeuroLab, Bergen,

Norway) for a voxel-by-voxel estimation of plasma volume obtained from phase-derived vascular input function and bookend T1 mapping (Vp_Φ) and volume transfer constant obtained from phase-derived vascular input function and bookend T1 mapping (K^{trans}_Φ). Postprocessing parameters were the following: noise level = 0, spatial smoothing = off, vascular deconvolution = on, normalize kinetic parameters = on, autodetect VIF-tissue delay = on, hematocrit correction factor = 0.45.

Magnitude-Derived Vascular Input Function with No T1 Correction. DCE magnitude images were processed directly in NordicICE to generate maps of plasma volume obtained from magnitude-derived vascular input function (Vp_SI) and volume transfer constant obtained from magnitude-derived vascular input function (K^{trans}_SI). The signal intensity (SI) was converted to percentage relative change in signal intensity (*relSI*) by using the expression: $relSI(t) = 100 \times (S(t) - S_o)/S_o$, where S is the SI at time t and S_o is the baseline SI. The *relSI* was assumed to be linearly related to concentration. The VIF was selected from a small ROI placed in the superior sagittal sinus directly from the DCE images. Signal conversion was set as SI to *relSI*(%). Other postprocessing parameters were similar to the analysis with phase-derived vascular input function and bookend T1 correction.

Postprocessing of DSC Images

DSC images were processed by using singular value decomposition and deconvolution as implemented in nordicICE. MR imaging signal intensity was converted to a T2 relaxation rate. An automated algorithm selected the most suitable pixels for VIF in a manually defined ROI covering the middle cerebral artery contralateral to the tumor. The SI was converted to relative change in R2 (ie, $R2^* = 1/T2^*$) by using the standard expression: $\Delta R2^*(t) = -\ln[S(t)/S_o]/TE$, where S is the SI at time t, S_o is the baseline SI, and TE is the echo time. Corrected CBV maps were generated. Correction for leakage in the CBV calculations was done by using preinjection of contrast agent and linear fitting to estimate the T1 contamination caused by extravasation of contrast agent.[13] Postprocessing parameters in nordicICE were the following: noise level = 0, no spatial smoothing, no temporal smoothing, signal conversion to $\Delta R2^*$, vascular deconvolution = on, apply contrast agent leakage correction = checked, detect both T1 and T2 leakage values = checked.

Image Interpretation

Two neuroradiologists (10 years of experience for C.H.T. and 12 years for S.C.) blinded to the histopathology determined the degree of tumoral contrast enhancement relative to the choroid plexus (none; mild [less than the choroid plexus]; moderate [equal to choroid plexus]; and marked [more than choroid plexus]). Axial T1-weighted postcontrast images were coregistered to the parametric maps. Because areas of highest values could vary between different parametric maps, a medical student traced 2 sets of ROIs: 1) 1 large "large-tumor" ROI over the solid component of the tumor for the section where the tumor was largest (identical ROI for all maps), and 2) 4 small "hot spot" ROIs (35 mm^2) over the areas of highest values, which could vary in location between maps. For each parametric map, the mean pixel value inside each of the 5 ROIs was calculated. For the 4 small hot spot ROIs, the 3 ROIs with the smallest values were discarded. Thus, for each parametric map, we recorded 2 values: 1 large-tumor value and 1 hot spot value. All ROIs were verified by a neuroradiologist to ensure that inadvertent placement on an adjacent vessel or hemorrhage was avoided. For DSC images, 2 sets of corrected CBV values were recorded for each patient: the unnormalized value (uCBV) and the value normalized to the contralateral white matter (rCBV).

Histopathologic Analysis

Following surgical resection or biopsy, histopathologic diagnosis was provided by neuropathologists (17 years of experience for J.W. and 21 years for G.H.J.) by using the 2007 World Health Organization classification. For each patient, a representative slide of the resected tumor tissue was selected by a neuropathologist (J.W.). Formalin-fixed, paraffin-embedded 4-μm-thick sections of representative tumor were stained immunohistochemically by using an antibody to the endothelial marker CD34 (CD34, monoclonal clone QBEND/10, catalog number PA0212, "ready-to use" antibody; Leica Biosystems; http://www.leicabiosystems.com), following antigen retrieval with citrate buffer pH 6.0 for 20 minutes. Detection of bound antibody was achieved by using the automated bond platform from Leica Biosystems. Whole-section slide digitalization was performed at ×20 by using a MiraxMidi microscope (Carl Zeiss; http://www.zeiss.com/corporate/en_de/home.html/). On visual inspection, 3 fields (0.5–2.5 mm^2) that appeared to have the darkest stain within the tumor were captured by using the software Pannoramic Viewer 1.15 (3DHistech; http://www.3dhistech.com/pannoramic_viewer). Images were imported into a computer-assisted image-analysis software for calculation of the MVD (number of vessels/mm^2) and MVA (vessel area/total field area) (Zen Blue 1.0; Carl Zeiss). For each patient, the highest MVD and MVA among the 3 fields were reported.

Statistical Analysis

Interobserver agreement on the degree of contrast enhancement was measured by using a κ statistic. Comparisons of immunohistochemical and DSC-/DCE-derived parameters according to the degree of contrast enhancement and tumor grade were performed by using the Kruskal-Wallis test and Mann-Whitney U test. Correlation analysis between DSC- and DCE-derived parameters with MVD and MVA was performed by using a Spearman rank correlation coefficient (r_s). All data were analyzed by using MedCalc (Version 12; MedCalc Software, Ostend, Belgium).

RESULTS

Forty-three patients with a new diagnosis of a glioma were included in this study. There were 10 patients with grade II gliomas (9 astrocytomas, 1 oligodendroglioma), 11 patients with grade III gliomas (6 astrocytomas, 4 oligoastrocytomas, 1 oligodendroglioma), and 22 patients with a glioblastoma (grade IV). Twenty-eight of these 43 patients were started on steroid therapy before their MR imaging examination. The mean age was 54 years (95% CI, 49.3–58.7 years). There were 21 men and 22 women.

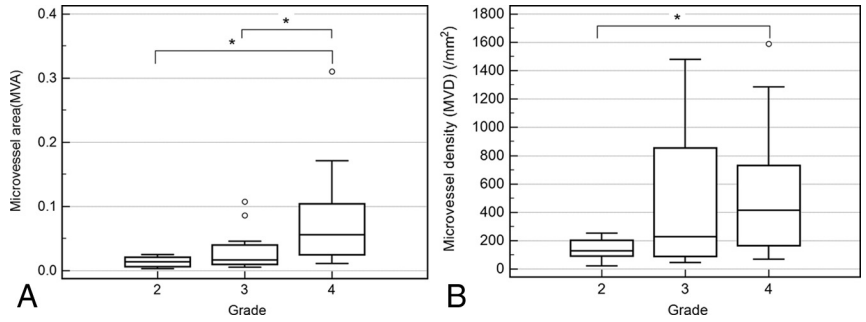

FIGURE. Box-and-whisker plots of microvessel area according to histopathologic grade (*A*) and microvessel density according to histopathologic grade (*B*). The *asterisk* indicates $P < .05$.

Table 1: Median values of MVA, MVD, and DCE- and DSC-MRI parameters with interquartile range for low and high-grade gliomas[a]

	Low-Grade (*n* = 10)	High-Grade (*n* = 33)	*P* Value
MVA (%)	1.4 (0.66–2.09)	3.2 (1.82–9.38)	.002
MVD (mm^2)	129 (93–202)	376 (157–768)	.006
Large-tumor Vp_Φ (%)	0.098 (0.01–0.58)	1.45 (0.71–2.21)	.001
Large-tumor Vp_SI (%)	0.69 (0.27–2.20)	3.12 (1.37–6.72)	.04
Large-tumor uCBV (a.u.)	35.8 (16.9–62.8)	80.8 (57.3–152.5)	.01
Large-tumor rCBV	2.9 (1.53–4.19)	5.43 (3.19–8.21)	.02
Large-tumor K^{trans}_Φ (min^{-1})	0.00016 (0.00001–0.00225)	0.019 (0.011–0.041)	.002
Large-tumor K^{trans}_SI (min^{-1})	0.0012 (0.0004–0.0137)	0.05 (0.0118–0.0773)	.004
Hot spot Vp_Φ (%)	0.46 (0.02–1.04)	2.93 (1.85–4.42)	.0004
Hot spot Vp_SI (%)	1.84 (1.13–3.39)	8.51 (4.14–13.80)	.015
Hot spot uCBV (a.u.)	40.2 (16.8–181.3)	163 (142–274)	.002
Hot spot rCBV	2.85 (1.75–7.45)	11.6 (6.48–18.50)	.008
Hot spot K^{trans}_Φ (min^{-1})	0.00054 (0.00017–0.01341)	0.047 (0.023–0.091)	.0006
Hot spot K^{trans}_SI (min^{-1})	0.016 (0.002–0.067)	0.095 (0.044–0.162)	.02

Note:—a.u. indicates arbitrary units.

[a] Interquartile ranges are in parentheses.

Table 2: Diagnostic accuracy of imaging and histopathologic parameters in differentiating grade III and IV astrocytomas using hot spot ROIs

Parameters	AUC	95% CI	Cutoff Value	Sensitivity (%)	Specificity (%)
MVA	0.78	0.60–0.90	<2.32	77	73
MVD	0.62	0.44–0.78	<103	95	36
Hot spot Vp_Φ	0.81	0.64–0.92	<1.88	91	73
Hot spot Vp_SI	0.66	0.47–0.81	<4.2	91	64
Hot spot uCBV	0.80	0.63–0.92	<141	86	73
Hot spot rCBV	0.70	0.51–0.85	<9.88	68	73
Hot spot K^{trans}_Φ	0.78	0.60–0.90	<0.024	86	64
Hot spot K^{trans}_SI	0.72	0.53–0.86	<0.056	82	64
Combined Vp_Φ + K^{trans}_Φ + MVA + uCBV	0.85	0.68–0.95	<0.67	77	82

Note:—AUC indicates area under the curve.

Immunohistologic and Kinetic Parameters According to Tumor Grade

For all gliomas, there was a positive correlation between MVA and MVD ($r_s = 0.74$; 95% CI, 0.57–0.85). For high-grade gliomas only, a similar positive correlation between MVA and MVD was found ($r_s = 0.73$; 95% CI, 0.52–0.86). Histopathologic grade was a factor influencing MVA and MVD according to the Kruskal-Wallis test of independent samples ($P < .05$, Figure). Post hoc pair-wise comparisons according to the Mann-Whitney *U* test showed that median values of MVA for grades II and III were statistically lower than those for grade IV ($P < .05$). Median MVA values were not statistically different between grades II and III ($P = .21$). Median MVD values were statistically lower for grade II compared with grade IV ($P = .02$) but were not statistically different between grades II and III and between grades III and IV ($P > .05$). MVA, MVD, DSC, and DCE parameters were significantly lower in low-grade-versus-high-grade gliomas (Table 1).

For differentiation between grade III and IV gliomas, there was a similar diagnostic accuracy between MVA (area under the curve = 0.78; 95% CI, 0.60–0.90), hot spot Vp_Φ (area under the curve = 0.81; 95% CI, 0.64–0.92), hot spot K^{trans}_Φ (area under the curve = 0.78; 95% CI, 0.60–0.90) and hot spot uCBV (area under the curve = 0.80; 95% CI, 0.63–0.92; Table 2). Combining those 4 parameters slightly improved the diagnostic accuracy (area under the curve = 0.85; 95% CI, 0.68–0.95).

MVA and MVD According to Tumor Enhancement

On postcontrast T1 images, there was excellent agreement between both radiologists in the assessment of gliomas that demonstrated no or mild enhancement versus those that demonstrated moderate or marked enhancement ($\kappa = 0.95$; 95% CI, 0.86–1). There was only 1 disagreement, which was settled by a third neuroradiologist. Among the 16 gliomas that had no or mild enhancement, 8 were low-grade, 7 were grade III, and 1 was grade IV. Among the 27 gliomas that demonstrated moderate or marked enhancement, there were 2 low-grade, 4 anaplastic grade III, and 21 grade IV gliomas. MVA and MVD were significantly higher in enhancing-versus-nonenhancing tumors or poorly enhancing tumors (Table 3).

Relationship between MVA and DSC- or DCE-Derived Parameters

The strongest correlation was found between MVA and large-tumor Vp_Φ ($r_s = 0.74$; 95% CI, 0.57–0.85; $P < .0001$; Table 4). The second strongest correlation was between MVA and hot spot Vp_Φ ($r_s = 0.69$; 95% CI, 0.49–0.82; $P < .0001$; Table 4). The correlation between MVA and hot spot uCBV ($r_s = 0.68$; 95% CI, 0.48–0.82; $P < .0001$) was stronger than that between MVA and hot spot rCBV ($r_s = 0.55$; 95% CI, 0.30–0.73; $P = .0001$). The correlation between MVA and large-tumor uCBV ($r_s = 0.61$; 95% CI, 0.37–0.77; $P < .0001$) was also stronger than that between MVA and large-tumor rCBV ($r_s = 0.50$; 95% CI, 0.23–0.69; $P = .0007$).

MVA correlated moderately with hot spot and large-tumor Vp_SI ($r_s = 0.44$; 95% CI, 0.16–0.65; and $r_s = 0.52$; 95% CI, 0.26–0.71, respectively; $P < .05$). MVA correlated moderately with hot spot and large-tumor K^{trans} values from both acquisition techniques (r_s between 0.54 and 0.57; $P \leq .0002$).

Table 3: Median values for MVA and MVD with interquartile ranges for nonenhancing/poorly enhancing gliomas and moderately/strongly enhancing gliomas[a]

Tumor Enhancement	MVA	MVD
None/poor ($n = 16$)	1.4% (0.68%–2.16%)	187 mm^2 (92–255 mm^2)
Moderate/strong ($n = 27$)	4.9% (2.08%–10.19%)	408 mm^2 (156–842 mm^2)
P value	.0002	.04

[a] Interquartile ranges are in parentheses.

Table 4: Correlations (r_s) among MVA, MVD, and DCE- and DSC-MRI parameters

Parameter	MVA (95% CI)	*P* Value	MVD (95% CI)	*P* Value
Large-tumor Vp_Φ	0.74 (0.57–0.85)	<.0001	0.52 (0.26–0.71)	.0003
Large-tumor Vp_SI	0.52 (0.26–0.71)	.0003	0.29 (−0.14–0.54)	.06
Large-tumor uCBV	0.61 (0.37–0.77)	<.0001	0.42 (0.14–0.64)	.005
Large-tumor rCBV	0.50 (0.23–0.69)	.0007	0.45 (0.18–0.66)	.002
Large-tumor K^{trans}_Φ	0.57 (0.33–0.75)	.0001	0.36 (0.07–0.60)	.02
Large-tumor K^{trans}_SI	0.56 (0.32–0.74)	.0001	0.41 (0.13–0.63)	.006
Hot spot Vp_Φ	0.69 (0.49–0.82)	<.0001	0.46 (0.18–0.66)	.002
Hot spot Vp_SI	0.44 (0.16–0.65)	.033	0.20 (−0.11–0.47)	.2
Hot spot uCBV	0.68 (0.48–0.82)	<.0001	0.48 (0.21–0.68)	.001
Hot spot rCBV	0.55 (0.30–0.73)	.0001	0.47 (0.20–0.68)	.002
Hot spot K^{trans}_Φ	0.56 (0.31–.74)	.0001	0.37 (0.073–0.60)	.02
Hot spot K^{trans}_SI	0.54 (0.29–0.73)	.0002	0.32 (0.024–0.57)	.04

Relationship between MVD and DSC- or DCE-Derived Parameters

There was a moderate correlation between MVD and large-tumor Vp_Φ ($r_s = 0.52$; 95% CI, 0.26–0.71; $P = .0003$; Table 4). MVD correlated moderately with normalized and unnormalized CBV for both hot spot and large-tumor ROIs (r_s between 0.42 and 0.48, $P < .05$). MVD correlated weakly with hot spot and large-tumor K^{trans} values (r_s between 0.32 and 0.41). No correlation was found between MVD and Vp_SI values ($P > .05$).

DISCUSSION

Quantification of angiogenesis by using vessel counting or vessel area has been found to be important for prognostication of patients with gliomas.[14,15] DSC- and DCE-MR imaging–derived tumor blood volume has been reported to be a prognostic and predictive marker for patients with gliomas.[1-5] Maps of blood volume or vascular permeability can also be generated across the whole tumor, allowing the neurosurgeon to determine preoperatively the most appropriate target for biopsy and/or resection. Validation of MR imaging–derived blood volume with microvessel area and density from immunohistochemistry is important because absolute CBV measurement is more difficult with MR imaging compared with CT. The relationship between MR imaging signal intensity and contrast concentration is not always linear. Multiple acquisition and postprocessing techniques can influence DCE- and DSC-derived tumor blood volume measurements.[5,6,13] For DSC-MR imaging, gradient-echo sequences are sensitive to vessels of all sizes, whereas spin-echo sequences are mainly sensitive to capillaries. Gradient-echo DSC-MR imaging can have large-vessel contamination. We tried to avoid this latter problem by drawing ROIs that avoided large vessels. For DCE-MR imaging, measurements of the VIF from magnitude images can have large systematic errors, which could lead to the underestimation of the contrast medium concentration. Phase images can provide a more accurate quantification of the VIF because the relationship between phase and contrast concentration remains linear, even at high concentrations.

Using both DCE- and DSC-MR imaging, we have shown that high-grade gliomas have higher cerebral blood volume, plasma volume, and K^{trans} compared with low-grade gliomas. This radiologic finding was confirmed by immunohistochemistry, which showed a higher microvessel density and microvessel area in high-grade gliomas versus low-grade gliomas. We also found that MVA correlated more with MR imaging–derived blood volume than MVD. Prior studies have shown a positive correlation between MVD and CBV obtained from perfusion CT or DCE-MR imaging in patients with gliomas.[16-19] In patients with recurrent high-grade gliomas, Hu et al[20] found that rCBV correlated strongly with MVA but weakly with MVD, in agreement with our study. Because high-grade gliomas in humans can display very heterogeneous vessels in terms of size, MVA has been found to be a better marker for angiogenesis than MVD because it encompasses both the number and size of microvessels.[14,20]

For DCE-MR imaging, a stronger correlation was found between MVA and Vp with a more quantitative approach with phase-derived VIF and pre- and postcontrast T1 mapping, compared with a simpler approach with magnitude-derived VIF without T1 mapping. The measurement of the VIF from magnitude images can be challenging due to numerous problems such as signal saturation at high contrast concentration and inflow effects. The use of phase rather than the magnitude signal can circumvent those artifacts and provide a more robust measurement of the VIF. The T1 mapping enables voxelwise determination of contrast agent concentration-versus-time in tumor tissue, which should improve the accuracy and standardization.[12] A moderate correlation was found between K^{trans} and MVA, regardless of the postprocessing techniques. This suggests that though K^{trans} is a more indirect marker of angiogenesis than Vp, it might be less influenced by differences in postprocessing techniques. In rats bearing C6 xenografts, with a magnitude-derived VIF, Ng et al[21] found that between-rat variance of K^{trans} measurements was lower than that for Vp. Jia et al[18] found a strong correlation between K^{trans} and CD105 MVD.

For DSC-MR imaging, the correlation between MVA and CBV was slightly weaker than that between MVA and DCE-derived Vp_Φ. The MVA-versus-CBV correlation was lower when CBV was normalized. For clinical applications, normalization of the CBV values against the contralateral white matter CBV has been recommended to obtain a relative CBV because for absolute quantification, the scaling factor converting signal intensity to contrast agent concentration is not known.[22,23] Normalization of CBV has been demonstrated to increase the repeatability of measurements, while arterial input function deconvolution may decrease it.[6] However, normalization also introduces noise in the measurements. An average coefficient of variation of 18% was

found for rCBV measurements of the normal-appearing white matter in 10 patients.[24] Some authors suggest using a median value of 3.2% for the normal-appearing white matter.[25] In our study, manual placement of the ROI in the contralateral white matter could have introduced an additional bias because the exact position might differ among patients. Hu et al[20] found excellent correlation between normalized CBV and MVA in recurrent gliomas. Their study differed from ours because they performed integration of the first-pass $\Delta R2^*$ curve to obtain CBV (without deconvolution). Hu et al also performed coregistration of rCBV measurements with stereotactic biopsy locations.

The main limitation of this study is the lack of coregistration between the ROI location on the parametric maps and the biopsy/resection tumor site from which the immunohistologic parameters were derived. In glioblastomas with heterogeneous enhancement, the lack of coregistration could lead to a poor correlation between MR imaging parameters and histology. Another source of sampling bias is the selection of fields for vessel quantification because only 3 small fields in the whole tumor specimen were selected for each patient. Use of CD105 might be a superior immunohistochemical marker for angiogenesis compared with CD34.[26] CD34 is prone to background staining and is a marker of endothelial cells for both immature and normal vessels. Finally, we performed multiple statistical comparisons without performing a Bonferroni correction. This could have led to a type I error (finding a difference that does not exist).

CONCLUSIONS

With DCE-MR imaging, use of a phase-derived VIF and bookend T1 mapping improves the correlation between immunohistochemistry and Vp (but not K^{trans}). With DSC-MR imaging, normalization of CBV could decrease correlation with the microvessel area.

Disclosures: Thanh Binh Nguyen—*RELATED*: *Grant*: Bayer Healthcare,* *Comments*: I received an investigator-initiated research grant; *Consulting Fee or Honorarium*: Bayer Healthcare, *Comments*: I have received consulting fees for my work with a perfusion expert panel; *Support for Travel to Meetings for the Study or Other Purposes*: Bayer Healthcare, *Comments*: I have received travel support from Bayer to cover hotel expenses to attend the perfusion imaging expert panel workshop; *UNRELATED*: *Consultancy*: Bayer Healthcare, *Comments*: I have acted as a consultant on a perfusion imaging panel; *Payment for Development of Educational Presentations*: Bayer Healthcare, *Comments*: I have participated in the development of a perfusion imaging syllabus. Kirstin Perdrizet—*RELATED*: *Grant*: Mach-Gaensslen Student Research Award,* *Comments*: This award was paid to my institution (University of Ottawa) for my studentship. John Woulfe—*UNRELATED*: *Grants/Grants Pending*: Physicians Services Incorporated Foundation,* *Comments*: For Parkinson disease research. *Money paid to the institution.

REFERENCES

1. Law M, Young RJ, Babb JS, et al. **Gliomas: predicting time to progression or survival with cerebral blood volume measurements at dynamic susceptibility weighted contrast-enhanced perfusion MR imaging.** *Radiology* 2008;247:490–98 CrossRef Medline
2. Hipp SJ, Steffen-Smith E, Hammoud D, et al. **Predicting outcome of children with diffuse intrinsic pontine gliomas using multiparametric imaging.** *Neuro Oncol* 2011;13:904–09 CrossRef Medline
3. Hirai T, Murakami R, Nakamura H, et al. **Prognostic value of perfusion MR imaging of high-grade astrocytomas: long-term follow-up study.** *AJNR Am J Neuroradiol* 2008;29:1505–10 CrossRef Medline
4. Mangla R, Singh G, Ziegelitz D, et al. **Changes in relative cerebral blood volume 1 month after radiation-temozolomide therapy can help predict overall survival in patients with glioblastoma.** *Radiology* 2010;256:575–84 CrossRef Medline
5. Nguyen TB, Cron GO, Mercier JF, et al. **Preoperative prognostic value of dynamic contrast-enhanced MRI-derived contrast transfer coefficient and plasma volume in patients with cerebral gliomas.** *AJNR Am J Neuroradiol* 2015;36:63–69 CrossRef Medline
6. Jafari-Khouzani K, Emblem KE, Kalpathy-Cramer J, et al. **Repeatability of cerebral perfusion using dynamic susceptibility contrast MRI in glioblastoma patients.** *Transl Oncol* 2015;8:137–46 CrossRef Medline
7. Khalifa F, Soliman A, El-Baz A, et al. **Models and methods for analyzing DCE-MRI: a review.** *Med Phys* 2014;41:124301 CrossRef Medline
8. van Osch MJ, Vonken EJ, Viergever MA, et al. **Measuring the arterial input function with gradient echo sequences.** *Magn Reson Med* 2003;49:1067–76 CrossRef Medline
9. Korporaal JG, van den Berg CA, van Osch MJ, et al. **Phase-based arterial input function measurements in the femoral arteries for quantification of dynamic contrast-enhanced (DCE) MRI and comparison with DCE-CT.** *Mag Reson Med* 2011;66:1267–74 CrossRef Medline
10. Foottit C, Cron GO, Hogan MJ, et al. **Determination of the venous output function from MR signal phase: feasibility for quantitative DCE-MRI in human brain.** *Magn Reson Med* 2010;63:772–81 CrossRef Medline
11. Nguyen TB, Cron GO, Perdrizet K, et al. **Comparison of the diagnostic accuracy of DSC- and dynamic contrast-enhanced MRI in the preoperative grading of astrocytomas.** *AJNR Am J Neuroradiol* 2015;36:2017–22 CrossRef Medline
12. Cron GO, Kelcz F, Santyr GE. **Improvement in breast lesion characterization with dynamic contrast-enhanced MRI using pharmacokinetic modeling and bookend T(1) measurements.** *Magn Reson Med* 2004;51:1066–70 CrossRef Medline
13. Boxerman JL, Schmainda KM, Weisskoff RM. **Relative cerebral blood volume maps corrected for contrast agent extravasation significantly correlate with glioma tumor grade, whereas uncorrected maps do not.** *AJNR Am J Neuroradiol* 2006;27:859–67 Medline
14. Korkolopoulou P, Patsouris E, Kavantzas N, et al. **Prognostic implications of microvessel morphometry in diffuse astrocytic neoplasms.** *Neuropathol Appl Neurobiol* 2002;28:57–66 CrossRef Medline
15. Wesseling P, van der Laak JA, Link M, et al. **Quantitative analysis of microvascular changes in diffuse astrocytic neoplasms with increasing grade of malignancy.** *Hum Pathol* 1998;29:352–58 CrossRef Medline
16. Jain R, Gutierrez J, Narang J, et al. **In vivo correlation of tumor blood volume and permeability with histologic and molecular angiogenic markers in gliomas.** *AJNR Am J Neuroradiol* 2011;32:388–94 CrossRef Medline
17. Haris H, Husain N, Singh A, et al. **Dynamic contrast-enhanced derived cerebral blood volume correlates better with leak correction than with no correction for vascular endothelial growth factor, microvascular density, and grading of astrocytoma.** *J Comput Assist Tomogr* 2008;32:955–65 CrossRef Medline
18. Jia ZZ, Gu HM, Zhou XJ, et al. **The assessment of immature microvascular density in brain gliomas with dynamic contrast-enhanced magnetic resonance imaging.** *Eur J Radiol* 2015;84:1805–09 CrossRef Medline
19. Sadeghi N, D'Haene N, Decaestecker C, et al. **Apparent diffusion coefficient and cerebral blood volume in brain gliomas: relation to tumor cell density and tumor microvessel density based on stereotactic biopsies.** *AJNR Am J Neuroradiol* 2008;29:476–82 CrossRef Medline
20. Hu LS, Eschbacher JM, Dueck AC, et al. **Correlations between perfusion MR imaging cerebral blood volume, microvessel quantification, and clinical outcome using stereotactic analysis in recurrent high-grade glioma.** *AJNR Am J Neuroradiol* 2012;33:69–76 CrossRef Medline

21. Ng CS, Wei W, Bankson JA, et al. **Dependence of DCE-MRI biomarker values on analysis algorithm.** *PLoS One* 2015;10:e0130168 CrossRef Medline
22. Shiroishi M, Castellazzi G, Boxerman JL, et al. **Principles of T2*-weighted dynamic susceptibility contrast MRI technique in brain tumor imaging.** *J Magn Reson Imaging* 2015;41:296–313 CrossRef Medline
23. Willats L, Calamante F. **The 39 steps: evading error and deciphering the secrets for accurate dynamic susceptibility contrast MRI.** *NMR Biomed* 2013;26:913–31 CrossRef Medline
24. Wetzel SG, Cha S, Johnson G, et al. **Relative cerebral blood volume measurements in intracranial mass lesions: interobserver and intraobserver reproducibility study.** *Radiology* 2002;224:797–803 CrossRef Medline
25. Kellner E, Breyer T, Gall P, et al. **MR evaluation of vessel size imaging of human gliomas: validation by histopathology.** *J Magn Reson Imaging* 2015;42:1117–25 CrossRef Medline
26. Nico B, Benagiano V, Mangieri D, et al. **Evaluation of microvascular density in tumors: pro and contra.** *Histol Histopathol* 2008;23:601–07 Medline